

A Halogen Bond Route to Shorten the Ultrashort Sextuple Bonds in Cr₂ and Mo₂

Jyothish Joy^a and Eluvathingal D. Jemmis^{*b}

^[a] Jyothish Joy

School of Chemistry, Indian Institute of Science Education and Research-Thiruvananthapuram, Kerala,
Thiruvananthapuram 695016, India.

^[b] Eluvathingal D. Jemmis

Department of Inorganic and Physical Chemistry, Indian Institute of Science, Bangalore 560012, India.

Supporting Information

* Corresponding author: Department of Inorganic and Physical Chemistry, Indian Institute of Science, Bangalore, 560012, India. Fax: 2360-1552; Tel: 080-2293-3347; E-mail: jemmis@ipc.iisc.ernet.in

Computational Details

Group 6 diatomic molecules (Cr_2 , Mo_2 , and W_2) possess the highest bond order (sextuple bond) and shortest metal-metal bond distances in the whole of the periodic table. The presence of 12 electrons in the metal-metal bonding region makes it difficult to describe the electronic structure correctly.¹ A recent study showed the impact of relativistic effects in breaking the periodicity of group 6 diatomics, where Cr_2 , Mo_2 , and W_2 possess sextuple bonding, and its higher analog Sg_2 possess quadruple bonding.² The multireference nature of these systems requires many configuration state functions to represent the correct electronic structure. However, a large number of studies showed that density functional theory calculations based on Generalized Gradient Approximation (GGA) functionals like PBE, BP86, and BLYP are capable of reproducing the correct bond length and bond dissociation energy of these molecules.²⁻³ We have used GGA-PBE functional with scalar relativistic zeroth-order regular approximation (SR-ZORA) Hamiltonian for geometry optimization and vibrational frequency calculation as implemented in ADF-2014 program package.⁴ Grimme's third order dispersion scheme (DFT-D3) is included to invoke the effect of dispersion in our calculations.⁵ All calculations are carried out using an all-electron Slater-type triple ζ - quality basis set, further designated as SR-ZORA-PBE-D3(BJ)/ae-TZVP.

The strength of halogen bonding ($\text{M}\cdots\text{I}$) and intrinsic interaction energy at the metal-metal sextuple bond are computed using energy decomposition analysis (EDA)⁶ and extended transition state – natural orbitals for chemical valence (ETS-NOCV) scheme⁷ as implemented in the ADF-2014 package. EDA decomposes the interaction energy into various physically meaningful quantities,

$$\Delta E_{\text{Int}} = \Delta E_{\text{Pauli}} + \Delta E_{\text{Electrostatics}} + \Delta E_{\text{orbital}} + \Delta E_{\text{Dispersion}}$$

ΔE_{Pauli} represents the pairwise exchange repulsion experienced by electrons of the same spin on either fragment, $\Delta E_{\text{Electrostatic}}$ is the quasi-classical electrostatic attraction between the fragments, $\Delta E_{\text{orbital}}$ stands for the orbital mediated charge transfer (CT) stabilization, and $\Delta E_{\text{Dispersion}}$ gives the stabilization component originated from the induced dipole interaction between the fragments.⁸

ETS-NOCV is capable of decomposing the $\Delta E_{\text{orbital}}$ term obtained from the EDA analysis further into the corresponding pairwise orbital components, which gives information about the magnitude and direction of electron density flow during the dimer formation from individual monomers.^{7b} We mostly depend on ETS-NOCV deformation density maps of the halogen bonded complexes to identify the direction and magnitude of electron density flow.⁹ Electron density difference (EDD) maps are also employed in this regard.¹⁰

The elusive nature of bonding in these highly correlated systems led Roos et al. to define the effective bond order (EBO), the difference between the number of electrons in bonding and antibonding natural orbitals divided by two, as the true measure of bond order instead of the conventional formal bond order (FBO).^{1b, 11} One may consider bond multiplicity as the lowest integer value larger than the EBO. Here, we calculated EBO using CASCSF(12,12) method as implemented in Gaussian-09 quantum chemistry package¹² using the optimized geometry from SR-ZORA-PBE-D3(BJ)/ae-TZVP. QTAIM topological

parameters are calculated using AIMALL package with the wave function files generated from the PBE-B3/Def2-TZVP calculations.¹³ Molecular electrostatic potential (MESP) maps are visualized using the GaussView software, and electron density difference (EDD) maps are computed using the Multiwfn program.¹⁰

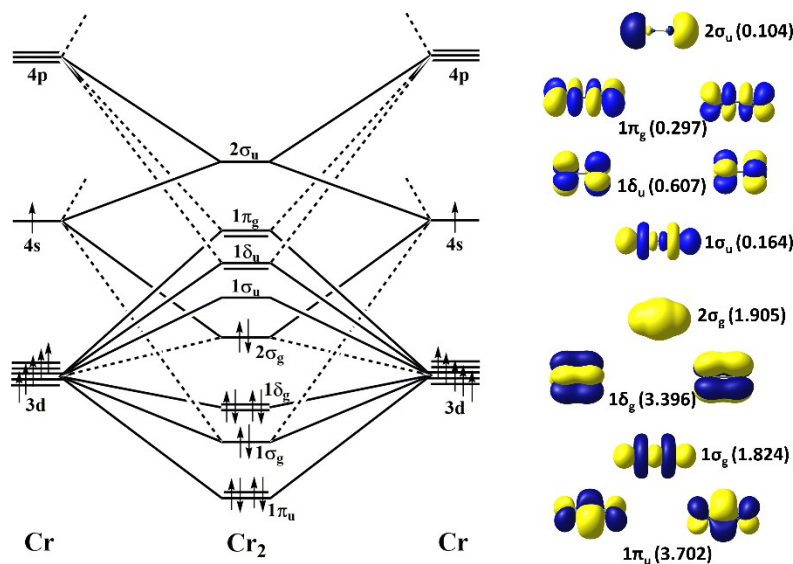


Figure S1. Orbital interaction diagram for the ${}^1\Sigma^+_g$ ground state of Cr_2 molecule. Relevant molecular orbitals and its corresponding natural orbital occupation numbers (NOON) from CASSCF(12,12) calculation are given.

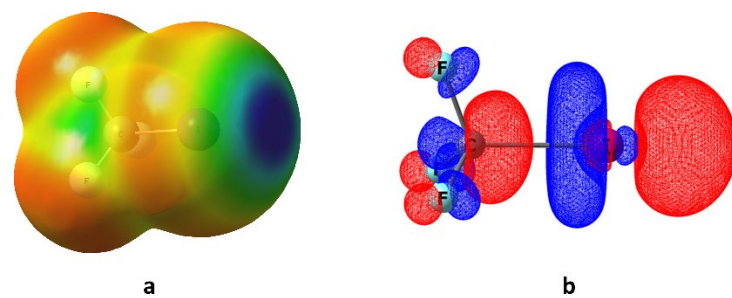


Figure S2. (a) Molecular electrostatic potential map (MESP) of CF_3I molecule showing the σ -hole at the iodine atom (blue region) and (b) the nature of its lowest unoccupied molecular orbital (LUMO).

Table S1. The strength of σ , π , and δ bonding components to the total orbital interaction energy of Cr_2 , Mo_2 and W_2 obtained from energy decomposition analysis at the metal-metal sextuple bond. Calculations are done at the SR-ZORA-PBE-D3(BJ)/ae-TZVP level of theory using ADF-2014 package.

Molecule	bond strength (kcal/mol)						
	$1\sigma_g$ (kcal/mol)	$2\sigma_g$ (kcal/mol)	σ_{total} (kcal/mol)	π_{total} (kcal/mol)	δ_{total} (kcal/mol)	Rest (kcal/mol)	Total orbital Interaction (kcal/mol)
Cr_2	-106.87	-7.03	-113.90	-172.87	-14.19	-1.62	-302.96
Mo_2	-105.84	-7.37	-113.21	-180.57	-22.07	-1.15	-317.96
W_2	-80.79	-17.26	-98.05	-165.73	-19.22	-1.47	-284.47

Table S2. Calculated bonding parameters for M_2 and $\text{F}_3\text{C}-\text{I}\cdots\text{M}-\text{M}\cdots\text{I}-\text{CF}_3$, $\text{M} = \text{Cr}$, Mo , and W , complexes. All the calculations, except the EBO from CASSCF(12,12), are calculated using ADF-2014 package at the SR-ZORA-PBE-D3(BJ)/ae-TZVP level of theory. CASSCF(12,12) calculations are carried out on the PBE optimized geometries using the Gaussian-09 package.

Complex	R_e (M-M) (Å)	v (cm ⁻¹)	D_e (kcal/mol)	EBO CASSCF(12,12)	FBO (NM/GJ)	DI (e)	d (I \cdots M) (Å)	BE/CF ₃ I (kcal/mol)
Cr_2	1.595	810.104	-35.92	4.83	6.11/6.01	6.13		
$\text{Cr}_2(\text{CF}_3\text{I})_2$	1.581	852.393	-39.50	4.13	5.39/5.32	5.29	2.754	-15.62
Mo_2	1.927	545.321	-93.37	5.15	6.14/6.01	6.11		
$\text{Mo}_2(\text{CF}_3\text{I})_2$	1.910	563.454	-98.55	4.53	5.39/5.32	5.32	2.905	-14.18
W_2	2.021	392.622	-114.32	5.18	6.08/6.01	6.09		
$\text{W}_2(\text{CF}_3\text{I})_2$	2.035	367.138	-109.72	5.13	5.43/5.39	5.42	2.883	-11.66

R_e = equilibrium metal-metal distance, v = metal-metal vibrational frequency, D_e = metal-metal bond dissociation energy, EBO and FBO = effective and formal bond orders, NM/GJ = Nalewajski-Mrozek and Gopinathan-Jug bond order analysis, DI = delocalization index calculated from QTAIM analysis, d(I \cdots M) = noncovalent halogen bonding distance, BE = binding energy of the halogen bond.

Table S3. Change in equilibrium bond length (ΔR_e), vibrational frequency (Δv), metal-metal bond energy (ΔE_{int}), effective and formal bond orders (EBO and FBO), and delocalization index (ΔDl) upon the formation of $CF_3I \cdots M \cdots ICF_3$ complexes, M=Cr, Mo, and W. All parameters are calculated using the formula [$\Delta X = X_{product} - X_{reactants}$]. Calculations are carried out at scalar relativistic ZORA-PBE-D3(BJ)/ae-TZ2P level of theory.

Complex	ΔR_e (M-M) (mÅ)	Δv (M-M) (cm ⁻¹)	Δv (C-I) (cm ⁻¹)	ΔE_{int} (M-M) ^a (kcal/mol)	Δ EBO ^b	Δ FBO ^c (NM/GJ)	ΔDl^d (e)
$Cr_2(CF_3I)_2$	-14.66	+42.29	-112.52	+3.58	-0.66	-0.72/-0.69	-0.84
$Mo_2(CF_3I)_2$	-17.00	+18.13	-107.77	+5.18	-0.62	-0.75/-0.69	-0.79
$W_2(CF_3I)_2$	+13.91	-25.48	-94.96	-4.60	-0.05	-0.65/-0.62	-0.67

(a) Positive values of ΔE_{int} represents metal-metal bond strengthening upon halogen bond formation; (b)EBO obtained from CASSCF(12,12)/Def2-TZVP calculations; (c) FBO obtained from Nalewajski-Mrozek(NM) and Gophinatan-Jug (GJ) bond order analysis; (d)Delocalization Index from QTAIM calculation; (e) BE per CF_3I values are calculated at ZORA-PBE-D3(BJ)/ae-QZ4P level of theory to minimize the basis set superposition error using the TZ2P optimized geometries.

Table S4. Natural orbital occupancy number in the valance natural orbitals of M_2 and $CF_3I \cdots M \cdots ICF_3$, M = Cr, Mo and W, from CASSCF(12,12) calculations.

Molecule	Cr_2	$Cr_2(CF_3I)_2$	Mo_2	$Mo_2(CF_3I)_2$	W_2	$W_2(CF_3I)_2$
π_g^*	0.297	0.285	0.194	0.178	0.178	0.185
$2\sigma_u^*$	0.164	0.134	0.110	0.095	0.131	0.138
$1\sigma_u^*$	0.104	0.815	0.088	0.763	0.081	0.069
δ_u^*	0.607	0.593	0.462	0.438	0.442	0.480
$2\sigma_g$	1.905	1.864	1.916	1.903	1.924	1.868
δ_g	3.396	3.409	3.538	3.564	3.548	3.510
$1\sigma_g$	1.824	1.185	1.886	1.238	1.874	1.934
π_u	3.702	3.715	3.806	3.821	3.822	3.814
EDO	4.83	4.17	5.15	4.53	5.18	5.13

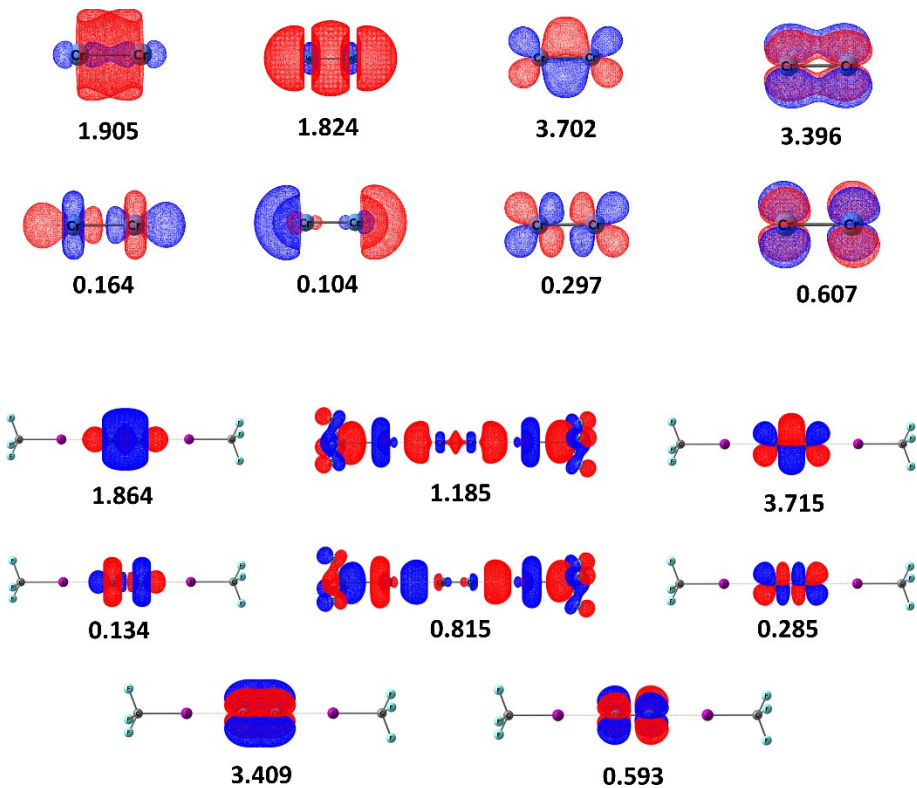


Figure S3. Natural orbitals and natural orbital occupation numbers from CASSCF(12,12) calculation for Cr_2 molecule and $\text{F}_3\text{Cl}\cdots\text{Cr}-\text{Cr}\cdots\text{ICF}_3$ complex.

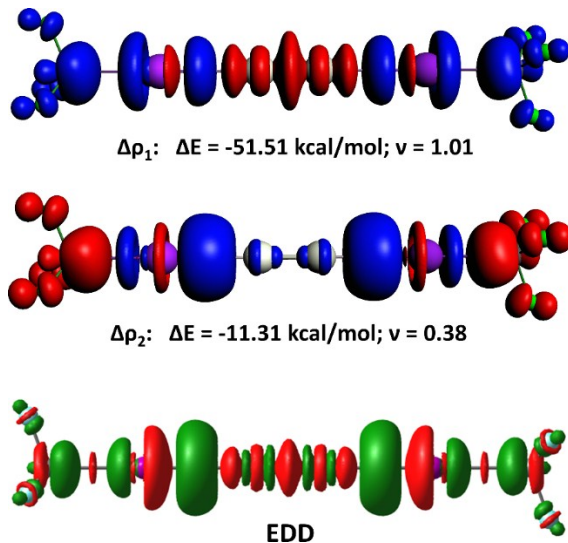


Figure S4. Two major components of the deformation density (Δp) for the complex $\text{F}_3\text{C}-\text{I}\cdots\text{Cr}-\text{Cr}\cdots\text{I}-\text{CF}_3$ obtained from scalar relativistic ZORA-PBE-D3(BJ)/ae-TZ2P calculations, where electron flow direction is from red→blue. The associated orbital interaction energy (ΔE) and size of the electron flow (v) are given. The total electron density difference (EDD) map is also given for comparison, where electron flow direction is from red→green.

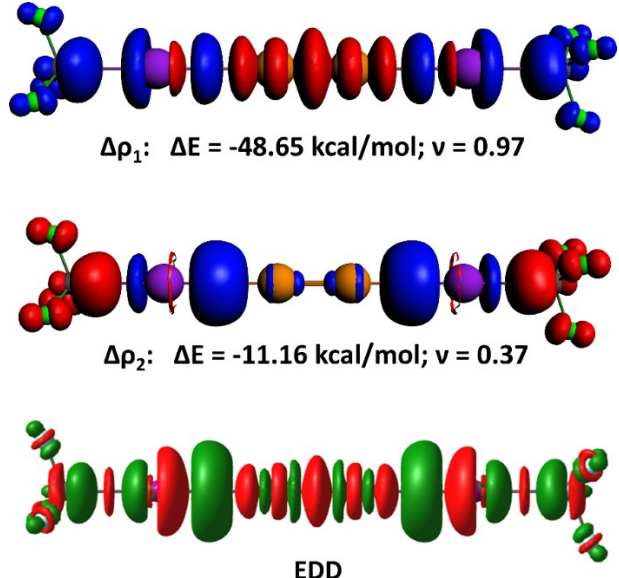


Figure S5. Two major components of the deformation density ($\Delta\rho$) for the complex $\text{F}_3\text{C}-\text{I}\cdots\text{Mo}=\text{Mo}\cdots\text{I}-\text{CF}_3$ obtained from scalar relativistic ZORA-PBE-D3(BJ)/ae-TZ2P calculations, where electron flow direction is from red \rightarrow blue. The associated orbital interaction energy (ΔE) and size of the electron flow (v) are given. The total electron density difference (EDD) map is also given for comparison, where electron flow direction is from red \rightarrow green.

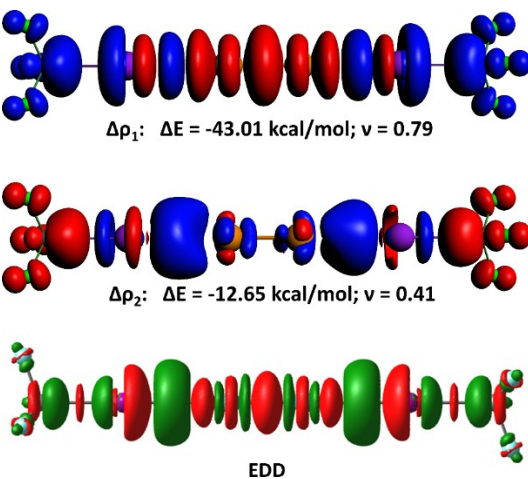


Figure S6. Two major components of the deformation density ($\Delta\rho$) for the complex $\text{F}_3\text{C}-\text{I}\cdots\text{W}=\text{W}\cdots\text{I}-\text{CF}_3$ obtained from scalar relativistic ZORA-PBE-D3(BJ)/ae-TZ2P calculations, where electron flow direction is from red \rightarrow blue. The associated orbital interaction energy (ΔE) and size of the electron flow (v) are given. The total electron density difference (EDD) map is also given for comparison, where electron flow direction is from red \rightarrow green.

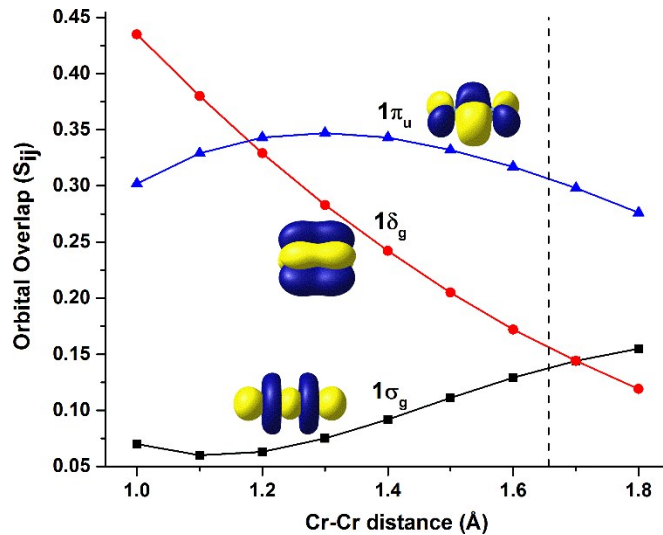


Figure S7. Variation in the orbital overlap (S_{ij}) as a function of Cr-Cr internuclear distance for $1\sigma_g^-$, $1\pi_u^-$, and $1\delta_g^-$ -bonding molecular orbitals. Vertical dashed line represents the S_{ij} value at the equilibrium bond length. The S_{ij} values are obtained using Slater-type orbitals.

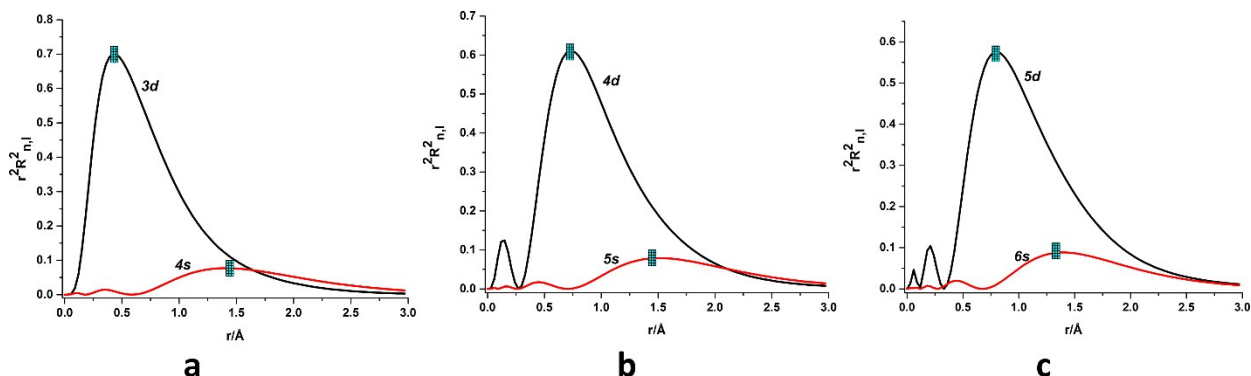


Figure S8: Radial density distribution $r^2 R(r)^2$ of nd, and (n+1)s orbitals for (a) chromium (n=3), (b) molybdenum (n=4) and (c) tungsten (n=5) from scalar relativistic DFT calculations using ZORA-PBE-D3(BJ)/ae-TZ2P level of theory. r = radial distance from the nucleus in angstrom unit.

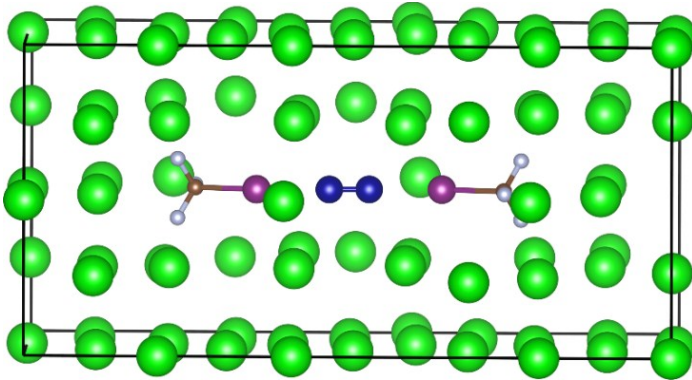


Figure S9. Optimized structure of the $\text{F}_3\text{C}-\text{I}\cdots\text{Cr}=\text{Cr}\cdots\text{I}-\text{CF}_3$ complex in explicit argon matrix. Calculations are done using periodic boundary conditions at the PBE-D3 level using VASP package.

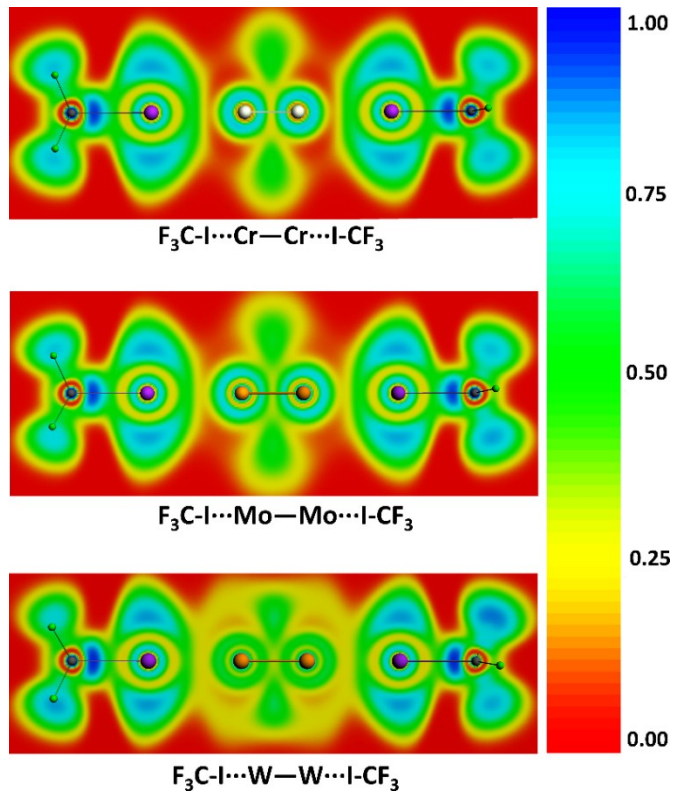


Figure S10. Electron localization function (ELF) of the complexes $\text{F}_3\text{C}-\text{I}\cdots\text{M}=\text{M}\cdots\text{I}-\text{CF}_3$, M = Cr, Mo, and W. The ELF represents the probability of locating electron pairs in the given molecule.

References

1. (a) B. O. Roos, *Collect. Czech. Chem. Commun.*, 2003, **68**, 265-274; (b) B. O. Roos, A. C. Borin and L. Gagliardi, *Angew. Chem., Int. Ed.*, 2007, **46**, 1469-1472; (c) A. C. Borin, J. P. Gobbo and B. O. Roos, *Chem. Phys. Lett.*, 2010, **490**, 24-28; (d) F. Ruipérez, G. Merino, J. M. Ugalde and I. Infante, *Inorg. Chem.*, 2013, **52**, 2838-2843.
2. Y.-L. Wang, H.-S. Hu, W.-L. Li, F. Wei and J. Li, *J. Am. Chem. Soc.*, 2016, **138**, 1126-1129.
3. (a) G. Merino, K. J. Donald, J. S. D'Acchioli and R. Hoffmann, *J. Am. Chem. Soc.*, 2007, **129**, 15295-15302; (b) K. E. Edgecombe and A. D. Becke, *Chem. Phys. Lett.*, 1995, **244**, 427-432; (c) E. J. Thomas Iii, J. S. Murray, C. J. O'Connor and P. Politzer, *Journal of Molecular Structure: THEOCHEM*, 1999, **487**, 177-182; (d) C. J. Barden, J. C. Rienstra-Kiracofe and H. F. Schaefer, *J. Chem. Phys.*, 2000, **113**, 690-700; (e) R. Würdemann, H. H. Kristoffersen, M. Moseler and M. Walter, *J. Chem. Phys.*, 2015, **142**, 124316.
4. G. te Velde, F. M. Bickelhaupt, E. J. Baerends, C. Fonseca Guerra, S. J. A. van Gisbergen, J. G. Snijders and T. Ziegler, *J. Comput. Chem.*, 2001, **22**, 931-967.
5. (a) T. Schwabe, S. Grimme and J.-P. Djukic, *J. Am. Chem. Soc.*, 2009, **131**, 14156-14157; (b) S. Grimme and J.-P. Djukic, *Inorg. Chem.*, 2010, **49**, 2911-2919; (c) U. Ryde, R. A. Mata and S. Grimme, *Dalton Trans.*, 2011, **40**, 11176-11183.
6. (a) T. Ziegler and A. Rauk, *Inorg. Chem.*, 1979, **18**, 1755-1759; (b) F. Bickelhaupt and E. Baerends, *Journal*, 2000.
7. (a) M. Mitoraj and A. Michalak, *J. Mol. Model.*, 2007, **13**, 347-355; (b) M. Mitoraj and A. Michalak, *Organometallics*, 2007, **26**, 6576-6580; (c) M. P. Mitoraj, A. Michalak and T. Ziegler, *J. Chem. Theory Comput.*, 2009, **5**, 962-975.
8. (a) G. Frenking and A. Krapp, *J. Comput. Chem.*, 2007, **28**, 15-24; (b) G. Frenking and F. Matthias Bickelhaupt, in *The Chemical Bond*, Wiley-VCH Verlag GmbH & Co. KGaA, 2014, DOI: 10.1002/9783527664696.ch4, pp. 121-157.
9. (a) J. Joy, E. D. Jemmis and K. Vidya, *Faraday Discuss.*, 2015, **177**, 33-50; (b) J. Joy and E. D. Jemmis, *Inorg. Chem.*, 2017, **56**, 1132-1143.
10. T. Lu and F. Chen, *J. Comput. Chem.*, 2012, **33**, 580-592.
11. A. C. Borin, J. P. Gobbo and B. O. Roos, *Chem. Phys.*, 2008, **343**, 210-216.
12. M. J. Frisch, G. W. Trucks, H. B. Schlegel, G. E. Scuseria, M. A. Robb, J. R. Cheeseman, G. Scalmani, V. Barone, B. Mennucci, G. A. Petersson, H. Nakatsuji, M. Caricato, X. Li, H. P. Hratchian, A. F. Izmaylov, J. Bloino, G. Zheng, J. L. Sonnenberg, M. Hada, M. Ehara, K. Toyota, R. Fukuda, J. Hasegawa, M. Ishida, T. Nakajima, Y. Honda, O. Kitao, H. Nakai, T. Vreven, J. A. Montgomery, J. E. Peralta, F. Ogliaro, M. Bearpark, J. J. Heyd, E. N. Brothers, K. N. Kudin, V. N. Staroverov, R. Kobayashi, J. Normand, K. Raghavachari, A. P. Rendell, J. C. Burant, S. S. Iyengar, J. Tomasi, M. Cossi, N. Rega, J. M. Millam, M. Klene, J. E. Knox, J. B. Cross, V. Bakken, C. Adamo, J. Jaramillo, R. Gomperts, R. E. Stratmann, O. Yazyev, A. J. Austin, R. Cammi, C. Pomelli, J. W. Ochterski, R. L. Martin, K. Morokuma, V. G. Zakrzewski, G. A. Voth, P. Salvador, J. J. Dannenberg, S. Dapprich, A. D. Daniels, Ö. Farkas, J. B. Foresman, J. V. Ortiz, J. Cioslowski and D. J. Fox, *Journal*, 2013, DOI: citeulike-article-id:9096580.
13. T. A. K. AIMAll (Version 16.01.09), TK Gristmill Software, Overland Park KS, USA, 2016 (aim.tkgristmill.com).

Cartesian coordinates of the optimized geometries

Cr₂

Cr	0.0000000000	0.0000000000	0.797676000
Cr	0.0000000000	0.0000000000	-0.797676000

F₃C—I···Cr—Cr···I—CF₃ Linear

Cr	0.0000000000	0.0000000000	0.790346000
Cr	0.0000000000	0.0000000000	-0.790346000
C	0.0000000000	0.0000000000	-5.934424000
C	0.0000000000	0.0000000000	5.934424000
I	0.0000000000	0.0000000000	-3.544826000
I	0.0000000000	0.0000000000	3.544826000
F	0.0000000000	-1.263633000	-6.385854000
F	1.094338000	0.631816000	-6.385854000
F	-1.094338000	0.631816000	-6.385854000
F	0.0000000000	1.263633000	6.385854000
F	1.094338000	-0.631816000	6.385854000
F	-1.094338000	-0.631816000	6.385854000

Mo₂

Mo	0.0000000000	0.0000000000	0.963408000
Mo	0.0000000000	0.0000000000	-0.963408000

F₃C—I···Mo—Mo···I—CF₃ Linear

Mo	0.000004000	0.000507000	0.954883000
Mo	0.000004000	-0.000507000	-0.954884000
C	-0.000005000	-0.000959000	6.228428000
C	-0.000005000	0.000960000	-6.228427000
I	0.0000000000	0.001056000	3.859885000
I	0.0000000000	-0.001056000	-3.859884000
F	-0.000006000	1.262176000	6.684190000
F	1.094187000	-0.633015000	6.682778000
F	-1.094200000	-0.633015000	6.682773000
F	-0.000006000	-1.262175000	-6.684190000
F	1.094187000	0.633015000	-6.682777000
F	-1.094199000	0.633016000	-6.682772000

W₂

W	0.0000000000	0.0000000000	1.010308000
W	0.0000000000	0.0000000000	-1.010308000

F₃C—I···W—W···I—CF₃ Linear

C	0.0000000000	-0.046231000	6.245646000
C	0.000008000	0.046361000	-6.245642000

I	0.000006000	0.050786000	3.900191000
I	-0.000006000	-0.050799000	-3.900192000
F	-0.000001000	1.196399000	6.752141000
F	1.094056000	-0.696502000	6.670558000
F	-1.094059000	-0.696501000	6.670553000
F	0.000010000	-1.196236000	-6.752217000
F	1.094068000	0.696658000	-6.670502000
F	-1.094047000	0.696660000	-6.670515000
W	-0.000002000	0.027980000	1.016880000
W	-0.000001000	-0.028029000	-1.016882000